ADVANCED FUNCTIONAL MATERIALS
www.afm-journal.de

Rational Design of Organic Semiconductors for Texture Control and Self-Patterning on Halogenated Surfaces

Jeremy W. Ward, Ruipeng Li, Abdulmalik Obaid, Marcia M. Payne, Detlef-M. Smilgies, John E. Anthony, Aram Amassian, and Oana D. Jurchescu**

Understanding the interactions at interfaces between the materials constituting consecutive layers within organic thin-film transistors (OTFTs) is vital for optimizing charge injection and transport, tuning thin-film microstructure, and designing new materials. Here, the influence of the interactions at the interface between a halogenated organic semiconductor (OSC) thin film and a halogenated self-assembled monolayer on the formation of the crystalline texture directly affecting the performance of OTFTs is explored. By correlating the results from microbeam grazing incidence wide angle X-ray scattering (μGIWAXS) measurements of structure and texture with OTFT characteristics, two or more interaction paths between the terminating atoms of the semiconductor and the halogenated surface are found to be vital to templating a highly ordered morphology in the first layer. These interactions are effective when the separating distance is lower than 2.5 d_w, where d_w represents the van der Waals distance. The ability to modulate charge carrier transport by several orders of magnitude by promoting "edge-on" versus "face-on" molecular orientation and crystallographic textures in OSCs is demonstrated. It is found that the "edge-on" self-assembly of molecules forms uniform, (001) lamellar-textured crystallites which promote high charge carrier mobility, and that charge transport suffers as the fraction of the "face-on" oriented crystallites increases.

1. Introduction

Solution processable organic semiconductors (OSCs) promise to allow mass-production of electronic devices at a low-cost, on flexible substrates such as plastics, paper and even on human skin.[1–5] The unique properties of such materials enable new paradigms for device manufacturing that go beyond the limitations of their a-Si:H counterpart and significantly reduce the cost and complexity of processing. For example, it has been shown that high performance organic single crystal and thin-film devices can be simultaneously deposited and patterned using ink-jet printing,[6,7] and that both the OSC and dielectric layers can be deposited in a one-step process by controlling their phase-separation from the mixed solution.[8,9] In these demonstrations, the relationship between the OSC and its interfaces within the device was successfully exploited to achieve the desired morphology. However, there is little insight into the roles of molecular design and interfacial interactions on molecular self-assembly in the context of heterogeneous nucleation at the solution-solid interface.[10] A recent development in this area is the successful use of fluorine–fluorine (F–F) interactions between the conjugated molecule and the surface to control crystallization and engineer film ordering.[11–15] Fluorine-terminated OSCs can exhibit a differential microstructure when deposited on surfaces selectively treated with fluorinated self-assembled monolayers (F-SAM): the formation of crystalline domains consisting of (001)-textured lamellar sheets of molecules, with in-plane π-stacking capable of effectively transporting charges at the semiconductor-dielectric interface, only occurs on and in the vicinity of regions where the F–F interactions are present. The surrounding regions exhibit a mixture of crystalline textures, which inhibit effective carrier transport, slowing it down by several orders of magnitude. The interface-driven growth behavior yields improved device performance by self-patterning the organic thin-film transistors (OTFTs) over an array of electrodes.[13,14] Our earlier investigations identified the role that the F–F interactions between the F-SAM and a fluorinated OSC have on the development of the crystalline order within the organic film and evaluated their strength with respect to the van der Waals intermolecular interactions.[12] However, the generality and the limitations of OTFT microstructural patterning via F–F interactions are not known. This insight is deemed crucial for the rational design of novel molecular structures coupled with surface treatments to enable high performance bottom-contact OTFT devices. The identification of appropriate

J. W. Ward, A. Obaid, Prof. O. D. Jurchescu
Department of Physics
Wake Forest University
Winston-Salem, NC 27109, USA
E-mail: jurchescu@wfu.edu
Dr. R. Li, Prof. A. Amassian
Division of Physical Sciences and Engineering
Solar and Photovoltaic Engineering Research Center
King Abdullah University of Science and Technology
Thuwal 23955, Saudi Arabia
E-mail: aram.amassian@kaust.edu.sa
Dr. M. M. Payne, Prof. J. E. Anthony
Department of Chemistry
University of Kentucky
Lexington, KY 40506, USA
Dr. D.-M. Smilgies
Cornell High Energy Synchrotron Source
Cornell University
Ithaca, NY 14850, USA

DOI: 10.1002/adfm.201400219

combinations of interfacial layers and OSCs can also assist in the development of cost-effective, bottom-up self-patterning procedures for organic electronic structures. We have therefore designed a series of experiments based on several combinations of F-SAMs and halogenated-OSCs to investigate F–F and F–S interactions. Displayed in **Figure 1** is the chemical structure of the OSCs we employed in this study: (a) diF-TES ADT (2,8- difluoro-5,11-bis(triethylsilylethynyl) anthradithiophene) referred to as ADT, (b) diF-TIPS Pn (a 1:1 isomeric mixture of 1,8- and 1,11-difluoro 6,13-bis(triisopropylsilylethynyl) pentacene) referred to as Pn, and (c) diF-TSBS PDT (2,10-difluoro-5,13-bis(tri-*sec*–butylsilylethynyl) pentadithiophene) referred to as PDT. Each of the above molecules crystallizes into lamellae with in-plane 2D-brickwork packing motif, which is necessary to achieve an "edge-on" co-facial packing within the OSC layer favoring 2D in-plane charge transport. The packing motif is crucial, as we have previously shown the interactions between the F-semiconductor and F-SAM are not sufficiently strong to modify the growth pattern of other packing motifs.[12,16,17] The ADT and PDT promote both F–F and F–S interactions with the F-SAM, while the Pn only allows the F–F interactions. This chemical difference offers us an experimental platform for the investigation of a secondary interaction, F–S, that was suggested to impact the microstructure within the organic films.[18] The length of the heteroacene backbone and its orientation with respect to the surface normal affect the distance between interacting terminal atoms and provide different interaction strengths for each of the three cases. The two F-SAMs, pentafluorobenzenethiol (PFBT) and 4-fluorobenzenethiol (4-MFBT), allow either one (4-MFBT) or multiple (PFBT) F–F interaction opportunities.

By correlating the crystalline texture from microbeam grazing incidence wide angle x-ray scattering (μGIWAXS) with electrical properties derived from OTFT measurements, we find that two conditions are necessary for successfully establishing the differential microstructure which promotes self-patterning and high electronic performance. First, at least two anchoring points must be established. These atoms originating from either the semiconductor or the F-SAM can connect with molecular moieties within the consecutive layer via F–F and/or F–S interactions. We believe this bonding, once established, can prevent any molecular twist in the first layer of the organic film and thus promotes the formation of a highly ordered templating layer. Second, when the separation between the interacting atoms is larger than about twice the sum of their van der Waals radii, the F–F and F–S interactions are too weak to dictate the polycrystalline texture within the film.

2. Results and Discussion

2.1. Structural Characterization

We have utilized μGIWAXS mapping, a method previously developed to map the microstructural heterogeneities of the OSC within OTFTs,[19] to determine the preferred microstructure and texture of the OSC on top of the untreated and F-SAM-treated Au electrodes and within the channel of the transistor, as shown in **Figure 2** and **Figure 3**. The treated Au surfaces maintain uniform, monolayer coverage for both F-SAMs, as suggested by our previous polarized modulated-infrared reflection absorption spectroscopy (PM-IRRAS), goniometric and Kelvin probe measurements.[12] As expected, all organic thin films were found to be highly crystalline. In the absence of a surface treatment, the crystalline texture of the semiconductor thin film consisted of a mixture of "edge-on" and "face-on"-oriented crystallites on the electrode and in the channel. However, the microstructure on the F-SAM-treated electrodes consisted of either purely "edge-on" oriented crystallites or of a mixture of orientations in various relative intensities (quantities), depending upon the choice of F-SAM, molecule and combination thereof, as will be discussed below. Note that for all three molecules, the "edge-on" molecular orientation presents the (001) texture, with the *a-b* plane and the π-stacking in the plane of the substrate, favoring good in-plane charge transport. On the contrary, the "face-on" orientation is geometrically ineffective for in-plane charge transport in OTFTs, present in the (111) texture of diF-TES ADT and (101) texture of diF-TIPS Pn and diF-TSBS PDT, respectively, as shown in Figure 3d–f. Mixtures of these two orientations also suffer from lower mobility, depending upon the relative amount of "face-on" oriented crystallites in the film.[12] Thus, self-patterning by differential microstructure is successful when the regions containing a pure (001) texture are present on the F-SAM-treated Au electrode and extend to its immediate vicinity (up to tens of microns) to completely cover the critical channel of the OTFT, and they are surrounded by regions consisting of a mixture of orientations. As all the molecules studied herein crystallized in mixed orientations on the

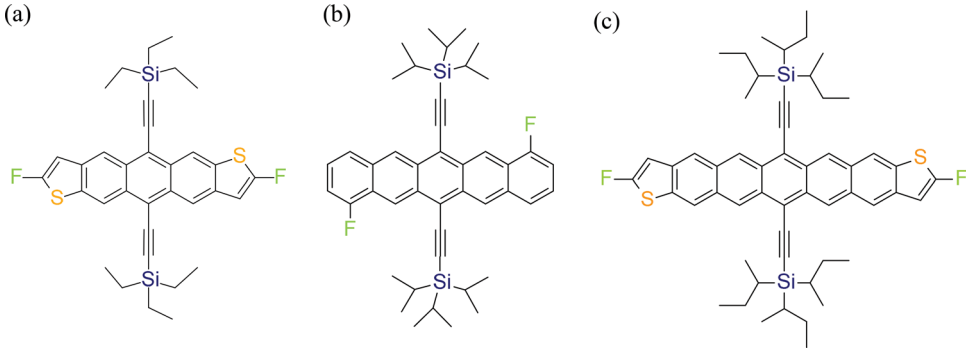

Figure 1. Chemical structures for (a) diF-TES ADT (ADT), (b) diF-TIPS Pn (Peri) (Pn), and (c) diF-TSBS PDT (PDT).

ADVANCED FUNCTIONAL MATERIALS
www.afm-journal.de

www.MaterialsViews.com

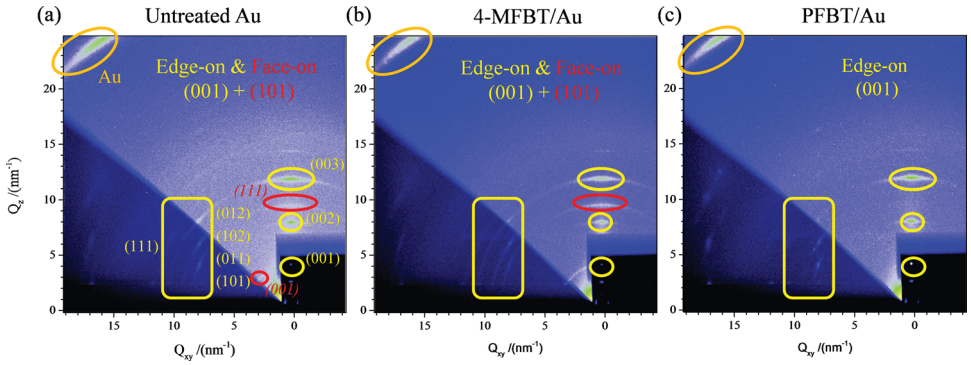

Figure 2. μGIWAXS patterns showing the diffraction pattern on films of Pn on (a) Untreated gold substrate, (b) 4-MFBT treated gold substrate, and (c) PFBT treated gold substrate. Peaks circled in yellow are associated with (001)-textured crystals, whereas the peaks identified by the red ovals are associated with (101)-textured crystals. A section of the intense Au (111) ring is also visible in the top left corner.

oxide regions located far from the electrodes, we will focus our comparison to the structural development directly on top of the F-SAM-treated Au electrodes. In Figure 2, we show representative μGIWAXS patterns for Pn on the electrode regions of the device (similar data was collected for ADT and PDT devices and the results are shown in Figure S1). Based on such scans on all material-SAM combinations (Figure 3), we have estimated the fraction of "edge-on" and "face-on" crystallite orientations across the entire device.[20]

In **Figure 4**a, we plotted the fraction of "edge-on" oriented crystallites for each combination of molecule/F-SAM. A summary of the film texture for each molecule-F-SAM combination is also summarized in **Table 1** and details about the determination of the fraction of "edge-on" orientation are provided in

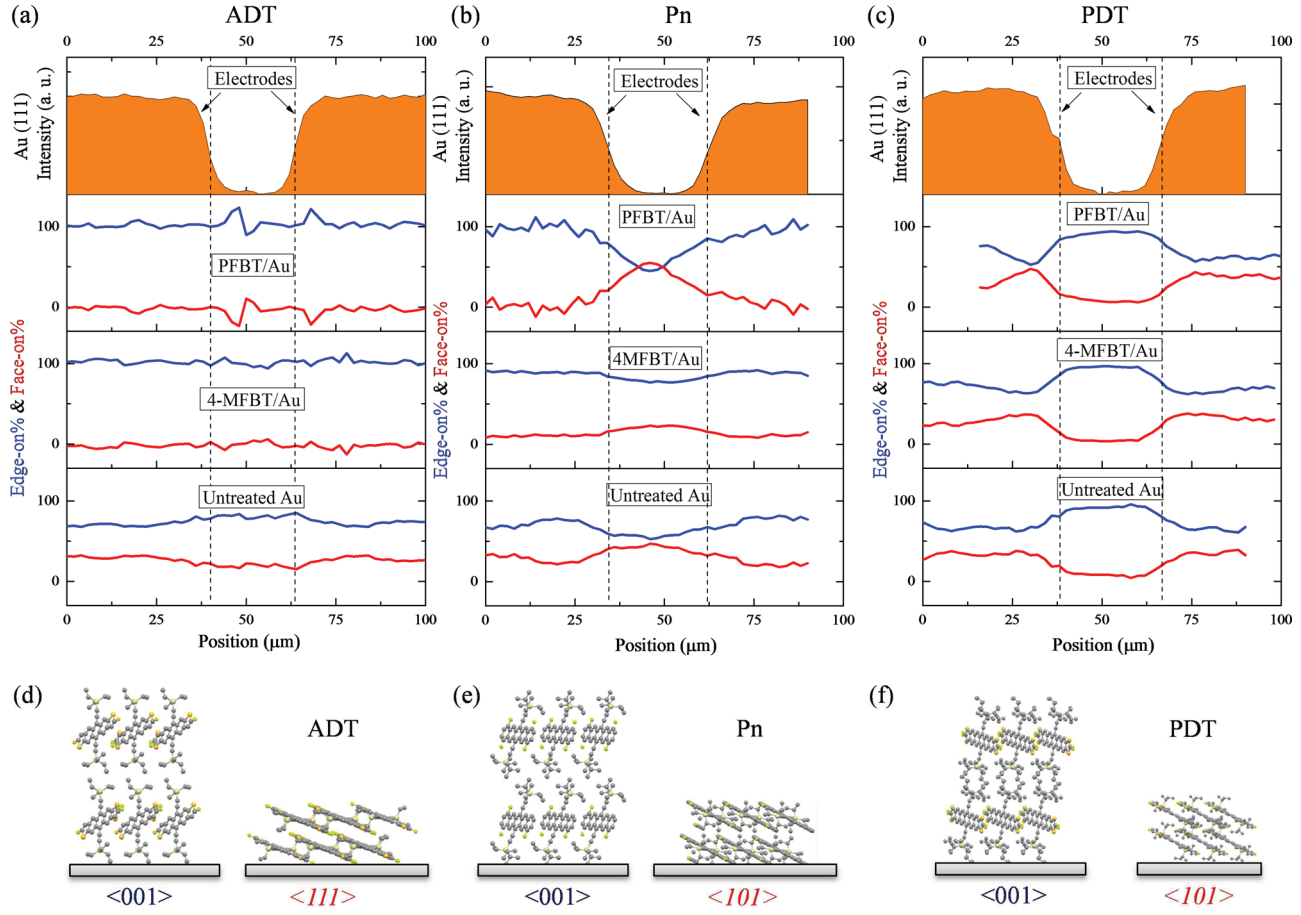

Figure 3. (a–c) Structural maps of bottom-contact OTFTs determined from μGIWAXS analysis. The top row of each figure denotes the gold electrodes and the bottom three rows denote the fractions of "edge-on" (blue) and "face-on" (red) orientations on PFBT/Au, 4-MFBT/Au, and untreated (UT) Au for (a) ADT, (b) Pn, and (c) PDT. (d–f) Schematic representations of the <001> and <111> molecular orientation for (d) ADT, (e) Pn and (f) PDT.

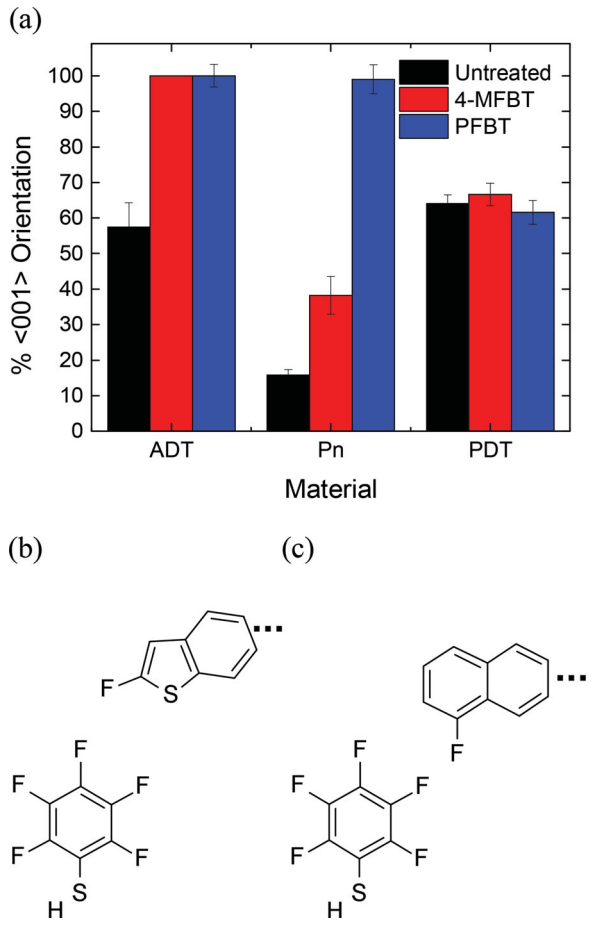

Figure 4. (a) Relative "edge-on" oriented content for ADT, PDT, and Pn deposited on PFBT (Blue), 4-MFBT (Red) and untreated substrates (Black). (b) Schematic illustrating the relationship between the OSC and the F-SAM for the cases when both F–F and F–S bonding present and (c) only F–F bonds are present.

Table S1. As expected, all the materials in question adopt a mixed orientation on untreated Au electrodes (black). In cases of the Pn and ADT molecules, the "face-on" orientation of crystallites is fully inhibited in thin films formed on PFBT/Au electrodes (blue). However, unlike ADT, Pn forms into a mixture of orientations when deposited on 4-MFBT/Au (red), despite the presence of the F–F interaction, suggesting that there is a threshold of minimum number of halogen bonds to influence molecular orientation and crystallographic texture. One F–F anchor, as in the case of Pn on 4-MFBT/Au, does not appear to be sufficiently strong to impede the growth of the "face-on" orientation. In the cases of Pn on PFBT and ADT on 4-MFBT or PFBT, there are multiple halogen bonding opportunities,

Table 1. Summary of crystalline orientations detected by μGIWAXS for different F-SAM/OSC combinations.

Material	PFBT	4-MFBT	Untreated
diF-TES ADT	(001)	(001)	(001) & (111)
diF-TIPS Pn (Peri)	(001)	(001) & (101)	(001) & (101)
diF-TSBS PDT	(001) & (111)	(001) & (101)	(001) & (101)

in the forms of F–F and/or F–S (Figures 4b,c), with the F/S atoms originating either from the SAM or the semiconductor. Such interactions can establish several active halogen bonds, obstructing molecular conformational changes and possibly anchoring the molecule onto the fluorinated surface in an orientation that favors growth of (001)-textured lamellar crystallites. The formation of 100% "edge-on" orientation of Pn crystallites on PFBT/Au suggests that two bonding opportunities are sufficient, here in the form of F–F interactions (Figure 4c), to successfully achieve a pure preferential orientation of the molecules at the surface of the treated electrodes. The single F–F path in the Pn/4-MFBT case, possibly together with "surface templating" provided by the aromatic SAM, encourages a higher content of "edge-on" crystallite orientation in Pn films on 4-MFBT/Au (28 ± 4.3%) compared to the case of untreated Au (10 ± 1.1%), but it is not sufficiently strong to promote the formation of a purely (001)-textured film, similar to the case of other OSC-SAM combinations.[21,22]

We now explore whether the formation of the pure (001) texture can be generalized for molecular systems containing F and S terminating atoms and deposited on an F-SAM surface. We performed similar measurements using PDT (Figure 1c), a molecule with a longer backbone, oriented at an 8.4° angle with respect to the surface normal. We found that in PDT, the presence of F-SAMs cannot suppress the formation of the (101) textured "face-on" orientation, even when several F–F and F–S anchors are afforded by the respective SAM and semiconductor molecular structures (Figure 4b). To understand these results we inspected in more detail the possible interactions at the F-SAM-OSC interface.

2.2. Interface Interactions Analysis

In **Figure 5**, we present a schematic view of the molecular orientation with respect to the substrate for a (001)-textured crystal viewed along the b-axis. The backbone orientation relative to the *a-b* plane is similar for each molecule and the angle with the substrate is provided in **Table 2**. The crystal structure was analyzed using CrystalMaker software.[23] We define the F–F and F–S separations, $d_{F\text{-}F}$ and $d_{F\text{-}S}$, as the distances between the F or S termination of the OSC molecule to the F termination of the SAM, which corresponds to a plane through the highest point of the F-SAM layer. This assumption is valid for both SAMs, as

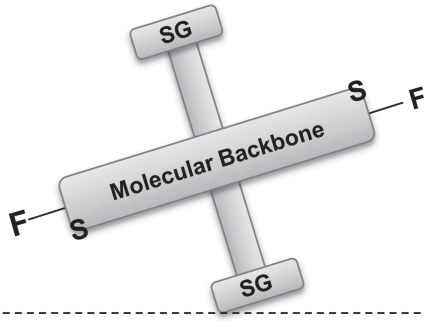

Figure 5. Schematic drawing of the relationship between the OSC backbone, substituent groups (SG) and the top of the F-SAM (represented as a dotted line).

Table 2. Comparison of Molecular Backbone to Substrate Angle and Relative Molecule-SAM Distances.

Material	Angle [°]	d_{F-F} [Å]	d_{F-S} [Å]
diF-TES ADT	20.7	5.13	5.13
diF-TIPS Pn (Peri)	2.5	4.49	–
diF-TSBS PDT	8.4	8.25	7.63

their orientations with respect to the surface normal are similar, with the aromatic ring slightly tilted with respect to the surface normal and the F-atom pointing upwards.[12] The distances for each compound are provided in Table 2. By correlating the estimated F–F and F–S separation distances with the experimental results provided in Figures 2,3 and 4, the current study provides a lower limit for the d_{F-F} and d_{F-S} for which the interaction is strong enough to promote long range order and inhibit the formation of the "face-on" oriented crystallites. We find that when the separation distance is $1.75 \cdot d_W$ or less, where d_W is the sum of the respective van der Waals radii, the formation of a pure "edge-on" orientation is observed for all cases explored herein.[24] This condition is achieved in the case of ADT and Pn molecules. In PDT the F–F and F–S interactions are weak as a result of relatively large separation induced by the backbone orientation ($\sim 2.5 \cdot d_W$). As a result, while the formation of (001)-oriented crystallites is observed, the presence of the F-SAM does not inhibit the formation of the "face-on" oriented crystallites. These results indicate the upper limit for the interaction distance lies within the range $1.75 \cdot d_W < d_{F-F/S} < 2.5 \cdot d_W$.

2.3. Electrical Characterization

Organic thin-film transistor measurements were performed as a means to investigate the impact of the film's microstructure and texture on the effectiveness of charge transport. In **Figure 6**, we show plots of the FET current-voltage characteristics: the evolution of the drain current versus the gate-source voltage ($\sqrt{I_D}$ versus V_{GS}) for representative devices of ADT (Figure 6a), Pn (Figure 6b) and PDT (Figure 6c) biased in the saturation regime (source-drain voltage, V_{DS} = –40 V). The evolution of the drain current versus the drain-source voltage for each semiconductor-treatment pair are shown in Figure S2. The graphs in Figure 6 correspond to untreated contacts (black), 4-MFBT (red), and PFBT treated (blue) electrodes, respectively. For all devices the channel lengths are sufficiently short that when the halogen interactions are effective, the crystallization induced from the electrodes into the channel inhibits the formation of "face-on" oriented crystallites.

The slope of the curves presented in Figure 6 yielded the field-effect mobility (μ) using the following relation:

$$\mu = \frac{2L}{WC_i}\left(\frac{\partial\sqrt{I_D}}{\partial V_{GS}}\right)^2 \quad (1)$$

where C_i = 17.3 nF cm^{-2} is the geometrical capacitance of the dielectric and L and W are the channel length and width,

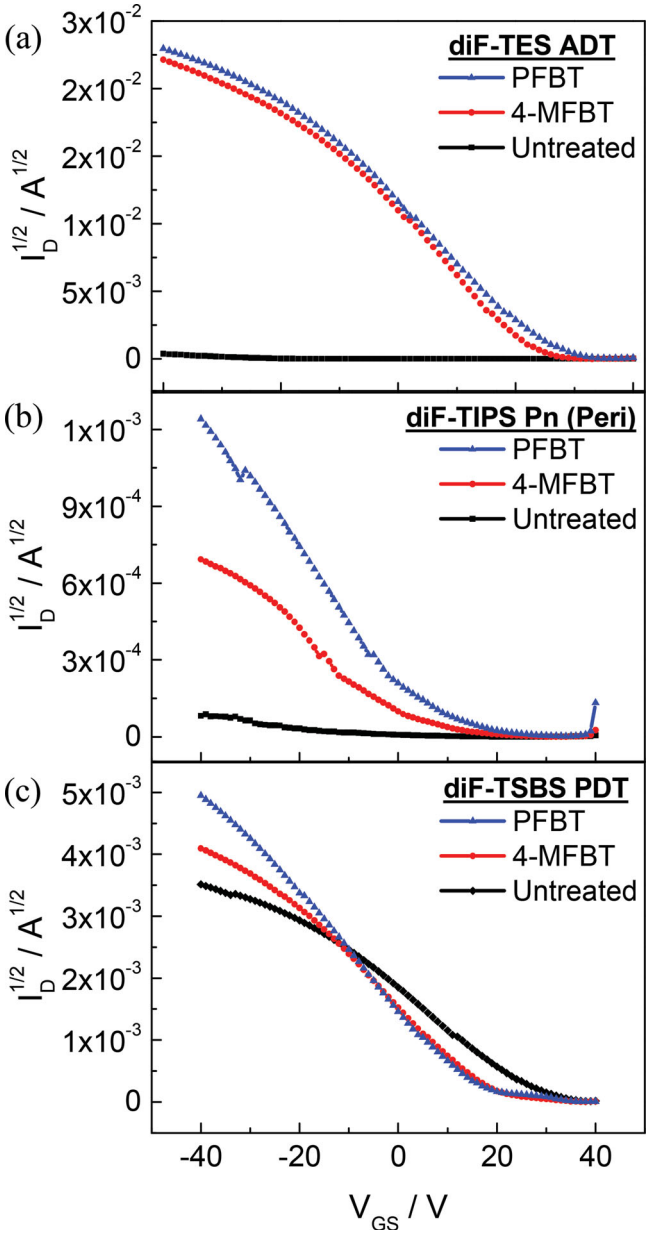

Figure 6. Evolution of the drain current, I_D, with gate voltage, V_{GS}, for (a) ADT, (b) Pn, and (c) PDT thin films on untreated (Black), 4-MFBT treated (Red), and PFBT treated (Blue) gold electrodes. The devices are measured at V_{DS} = –40 V with a transistor geometry of L = 5 μm (ADT) or L = 15 μm (Pn and PDT), W = 1000 μm, and oxide thickness of t_{ox} = 200 nm.

respectively. The reported averages were calculated based on the results obtained on at least 5 devices. Devices fabricated on ADT films deposited on PFBT and 4-MFBT treated electrodes showed high currents and produced similar mobilities of $\mu_{PFBT/Au} = (1.23 \pm 0.09) \times 10^{-1}$ cm^2 V^{-1} s^{-1} and $\mu_{4\text{-}MFBT/Au} = (9.7 \pm 1.2) \times 10^{-2}$ cm^2 V^{-1} s^{-1}, respectively. Films deposited on untreated electrodes exhibited nearly two orders of magnitude poorer performance, with $\mu_{Au} = (1.8 \pm 0.5) \times 10^{-3}$ cm^2 V^{-1} s^{-1}. The lower mobility is a result of higher injection barrier at the metal/OSC interface in the absence of the F-SAM, and due to the presence of the mixed molecular orientations, with the

"face-on" (111)-oriented crystallites hindering in-plane charge transport and intergrain transport due to large crystallographic misorientation.[12]

Measurements performed on devices fabricated using Pn films also echo the differences determined in our structural studies: the OTFTs fabricated on PFBT-treated electrodes showed the highest mobility with $\mu_{PFBT/Au} = (2.1 \pm 0.2) \times 10^{-3}$ cm^2 V^{-1} s^{-1}, owing to a pure "edge-on" molecular orientation obtained in the presence of favorable F–F interactions. Pn-based devices on 4-MFBT-treated electrodes and on untreated electrodes showed progressively decreasing performances due to the decrease in the amount of (001)-textured crystallites phase content (Figure 3b). The resulting values for mobilities are $\mu_{4\text{-}MFBT/Au} = (7.6 \pm 0.4) \times 10^{-4}$ cm^2 V^{-1} s^{-1} and $\mu_{Au} = (9 \pm 8) \times 10^{-6}$ cm^2 V^{-1} s^{-1} for devices based on 4-MFBT-treated and untreated electrodes, respectively.

When the separation distance between the semiconducting molecule and the F-SAM is too large to promote halogen-halogen interactions, such as in the PDT case, then μGIWAXS shows a mixture of orientations on all electrodes and OTFT devices also yield similar electrical properties for all types of electrodes. The characteristic mobilities measured for PDT films are: $\mu_{PFBT/Au} = (1.8 \pm 0.4) \times 10^{-2}$ cm^2 V^{-1} s^{-1}, $\mu_{4\text{-}MFBT/Au} = (1.1 \pm 0.3) \times 10^{-2}$ cm^2 V^{-1} s^{-1}, and $\mu_{Au} = (8.0 \pm 0.7) \times 10^{-3}$ cm^2 V^{-1} s^{-1}. The slightly higher mobilities obtained on PFBT/Au and 4-MFBT/Au are a result of the lower injection barrier created by the work function shift of the F-SAM-treated electrode.[12] Nevertheless, these values are significantly lower than the one reported for PDT OTFTs deposited by solvent-assisted crystallization (SAC), where a pure (001) oriented film, characterized by $\mu = 1.5$ cm^2 V^{-1} s^{-1} was obtained because of the slow nature of this crystallization process.[25] The lower mobility in our thin-films is thus limited by injection into (001) + (111) phase and not by the transport through the (001) phase present in the channel (Figure 3).[12]

3. Conclusions

We have investigated the role of interfacial halogenation of the substrate on mediating texture formation and self-patterning of polycrystalline OSC films and the resulting effects on charge transport properties in OTFTs. We demonstrate that OSCs can either allow or inhibit texture selection based on whether or not F–F and/or F–S interactions are present at the F-SAM/semiconductor interface. We report that the presence of two or more interaction opportunities between F and F/S species per SAM or per OSC molecule are required to promote molecular anchoring, which facilitates the formation of high in-plane mobility textures of the OSC. The halogen interactions are found to be sufficiently strong to mediate texture only when the halogen atoms on the molecule and the SAM are located closer than about twice the respective van der Waals interaction distances. When these conditions are satisfied, the organic film exhibits a high degree of texture purity, with crystallites oriented with the (001) plane parallel to the surface and effective in-plane π-stacking, resulting in high mobility devices. This study has provided rare insight directly linking the surface chemistry of the electrode, the terminating atom of the OSC molecules, the resulting film microstructure and the performance of OTFT devices. This information is vital to enabling the rational design of OSCs and demonstrates the importance of considering both the molecule and surface chemistry.

4. Experimental Section

Self-Assembled Monolayer Treatment: SAM treatment solutions were prepared by dissolving the respective molecules in ethanol (Sigma Aldrich). The treatment consisted of soaking the substrate for 30 min in a 30 mM room-temperature solution followed by a 5 min sonication in an ethanol bath for removal of the bulk layers. The substrates were then rinsed with ethanol and dried using a stream of N_2 gas.

Field-Effect Transistor Fabrication and Characterization: The device characterization was carried out using bottom contact OTFT structures on a highly doped Si gate electrode with a 200 nm thermally grown SiO_2 gate dielectric. The source and drain contacts (5 nm Ti/45 nm Au) were defined by optical photolithography and deposited by e-beam evaporation. The substrates were cleaned in hot acetone and isopropanol, followed by a 10 min UV-ozone exposure, ethanol rinse, and N_2 drying. The SAM layers were subsequently applied, as described in the previous section. The OSCs were synthesized following the procedures previously reported and were dissolved in a 1.2 wt% solution in high purity chlorobenzene (Sigma Aldrich).[26,27] The warm (55 °C) solution was spin cast onto the substrates at a 1000 rpm spinning speed and the obtained films were placed in a vacuum oven at room-temperature for 24 h to ensure full solvent removal. The devices were electrically characterized in a nitrogen environment using an Agilent 4155C Semiconductor parameter analyzer.

μGIWAXS Mapping of OTFT Devices: μGIWAXS measurements were performed at D-line, Cornell High Energy Synchrotron Source (CHESS) at Cornell University. The x-ray beam with a wavelength of 1.155 Å and a wide bandpass (1.47%) was focused into a 10 × 10 μm^2 spot using a single-bounce X-ray focusing capillary positioned on a V groove. The samples were placed on the focal point of the capillary (35 mm away from the capillary tip) and an incidence angle of 2° was chosen to ensure the beam footprint did not extend beyond the channel width of individual OTFTs. An optical microscope was located vertically on top of the sample and was used to monitor the beam and sample locations using a positionally calibrated crosshair. The beam footprint was imaged using a polished CdWO_3 crystal as fluorescence target. A square beam attenuator was placed between the sample and the detector to weaken 5 times of the intense (001) Bragg sheet in the (001) texture, thus allowing longer integration times for other diffraction peaks without saturating the detector. A Medoptics CCD detector located 98 mm from the sample holder was used with an exposure time of 30 s and a lateral sample scan step of 2 μm to collect μGIWAXS maps of each device according to a mapping procedure previously developed elsewhere.[19]

Supporting Information

Supporting Information is available from the Wiley Online Library or from the author.

Acknowledgements

The work at WFU was supported by the NSF grant ECCS-1102275. JWW gratefully acknowledges financial support from the NSF Graduate Student Fellowship (Grant No. DGE-0907738). Work at UKY was supported by the NSF grant CMMI-1255494. Part of this work was performed at the Cornell High Energy Synchrotron Source supported by the National Science Foundation and NIH-NIGMS via NSF award DMR-0936384.

Received: January 21, 2014
Revised: March 21, 2014
Published online: May 15, 2014

[1] T. Someya, T. Sekitani, S. Iba, Y. Kato, H. Kawaguchi, T. Sakurai, G. M. Whitesides, *Proc. Natl. Acad. Sci. USA* **2010**, *101*, 9966.
[2] H. Yan, Z. Chen, Y. Zheng, C. Newman, J. R. Quinn, F. Dötz, M. Kastler, A. Facchetti, *Nature* **2009**, *457*, 679.
[3] Y. Chung, B. Murmann, S. Selvarasah, M. R. Dokmeci, Z. Bao, *Appl. Phys. Lett.* **2010**, *96*, 133306.
[4] P. J. Diemer, C. R. Lyle, Y. Mei, C. Sutton, M. M. Payne, J. E. Anthony, V. Coropceanu, J.-L. Brédas, O. D. Jurchescu, *Adv. Mater.* **2013**, *25*, 6956.
[5] Y. Mei, M. A. Loth, M. Payne, W. Zhang, J. Smith, C. S. Day, S. R. Parkin, M. Heeney, I. McCulloch, T. D. Anthopoulos, J. E. Anthony, O. D. Jurchescu, *Adv. Mater.* **2013**, *25*, 4352.
[6] H. Minemawari, T. Yamada, H. Matsui, J. Tsutsumi, S. Haas, R. Chiba, R. Kumai, T. Hasegawa, *Nature* **2011**, *475*, 364.
[7] T. N. Ng, S. Sambandan, R. Lujan, A. C. Arias, C. R. Newman, H. Yan, A. Facchetti, *Appl. Phys. Lett.* **2009**, *94*, 233307.
[8] L. Qiu, J. A. Lim, X. Wang, W. H. Lee, M. Hwang, K. Cho, *Adv. Mater.* **2008**, *20*, 1141.
[9] C. Liu, T. Minari, X. Lu, A. Kumatani, K. Takimiya, K. Tsukagoshi, *Adv. Mater.* **2011**, *23*, 523.
[10] R. Li, H. U. Khan, M. M. Payne, D.-M. Smilgies, J. E. Anthony, A. Amassian, *Adv. Funct. Mater.* **2013**, *23*, 291.
[11] K. Reichenbächer, H. I. Süss, J. Hulliger, *Chem. Soc. Rev.* **2005**, *34*, 22.
[12] J. W. Ward, M. A. Loth, R. J. Kline, M. Coll, C. Ocal, J. E. Anthony, O. D. Jurchescu, *J. Mater. Chem.* **2012**, *22*, 19047.
[13] D. J. Gundlach, J. E. Royer, S. K. Park, S. Subramanian, O. D. Jurchescu, B. H. Hamadani, A. J. Moad, R. J. Kline, L. C. Teague, O. Kirillov, C. A. Richter, J. G. Kushmerick, L. J. Richter, S. R. Parkin, T. N. Jackson, J. E. Anthony, *Nat. Mater.* **2008**, *7*, 216.
[14] R. J. Kline, S. D. Hudson, X. Zhang, D. J. Gundlach, A. J. Moad, O. D. Jurchescu, T. N. Jackson, S. Subramanian, J. E. Anthony, M. F. Toney, L. J. Richter, *Chem. Mater.* **2011**, *23*, 1194.
[15] S. M. Huston, J. Wang, M. A. Loth, J. E. Anthony, B. R. Conrad, D. B. Dougherty, *J. Phys. Chem. C* **2012**, *116*, 21465.
[16] J. Chen, S. Subramanian, S. R. Parkin, M. Siegler, K. Gallup, C. Haughn, D. C. Martin, J. E. Anthony, *J. Mater. Chem.* **2008**, *18*, 1961.
[17] O. D. Jurchescu, B. H. Hamadani, H. D. Xiong, S. K. Park, S. Subramanian, N. M. Zimmerman, J. E. Anthony, T. N. Jackson, D. J. Gundlach, *Appl. Phys. Lett.* **2008**, *92*, 132103.
[18] Y. Wang, S. R. Parkin, J. Gierschner, M. D. Watson, *Org. Lett.* **2008**, *10*, 3307.
[19] R. Li, J. W. Ward, D.-M. Smilgies, M. M. Payne, J. E. Anthony, O. D. Jurchescu, A. Amassian, *Adv. Mater.* **2012**, *24*, 5553.
[20] E. J. Kintzel, D.-M. Smilgies, J. G. Skofronick, S. A. Safron, D. H. Van Winkle, *J. Cryst. Growth* **2006**, *289*, 345.
[21] C. H. Kim, H. Hlaing, F. Carta, Y. Bonnassieux, G. Horowitz, I. Kymissis, *ACS Appl. Mater. Interfaces* **2013**, *5*, 3716.
[22] H. Lee, Y. Zhang, L. Zhang, T. Mirabito, E. K. Burnett, S. Trahan, A. R. Mohebbi, S. C. B. Mannsfeld, F. Wudle, A. L. Briseno, *J. Mater. Chem. C* **2014**23361.
[23] D. Palmer, Crystal Maker (ver. 2.5), http://www.crystalmaker.com/, accessed May, 2014.
[24] A. Bondi, *J. Phys. Chem.* **1964**, *68*, 441.
[25] K. P. Goetz, Z. Li, J. W. Ward, C. Bougher, J. Rivnay, J. Smith, B. R. Conrad, S. R. Parkin, T. D. Anthopoulos, A. Salleo, J. E. Anthony, O. D. Jurchescu, *Adv. Mater.* **2011**, *23*, 3698.
[26] M. M. Payne, S. A. Odom, S. R. Parkin, J. E. Anthony, *Org. Lett.* **2004**, *6*, 3325.
[27] S. Subramanian, S. K. Park, S. R. Parkin, V. Podzorov, T. N. Jackson, J. E. Anthony, *J. Am. Chem. Soc.* **2008**, *130*, 2706.